Received: 3 January 2020 | Revised: 23 February 2020 | Accepted: 8 March 2020

DOI: 10.1111/jace.17107

Journal of the American Ceramic Society

ORIGINAL ARTICLE

Influence of surface orientation on the photochemical reactivity of $CaTiO_3$

Kayla E. Zitello | **Paul A. Salvador** | **Gregory S. Rohrer**

Department of Materials Science and Engineering, Carnegie Mellon University, Pittsburgh, PA, USA

Correspondence
Gregory S. Rohrer, Department of Materials Science and Engineering, Carnegie Mellon University, Pittsburgh, PA 15213, USA.
Email: gr20@andrew.cmu.edu

Funding information
National Science Foundation, Grant/Award Number: DMR 1609369; Carnegie Mellon University, Grant/Award Number: MCF-677785

Abstract

The orientations and surface structures of ferroelastic $CaTiO_3$ crystals within a polycrystalline ceramic were measured by electron backscatter diffraction and atomic force microscopy (AFM) respectively. Surfaces annealed at 1250°C in air are made up of a combination of facets with orientations near {100}, {110}, and {111} (indexed with reference to the cubic perovskite cell). The samples were immersed in an aqueous $AgNO_3$ solution and illuminated to photochemically reduce silver. Based on the amount of silver reduced on different surfaces, it was determined that surfaces with a {111} orientation had the greatest photocathodic reactivity, those with a {110} orientation had the least photocathodic reactivity, and surfaces with the {100} orientation had intermediate reactivity. While the {110} surfaces were essentially inert for photocathodic reduction, they were active for the photoanodic oxidation of Mn^{2+}. Ferroelastic domains were observed to enhance and retard the photochemical reduction of silver on spatially alternating domains on 20% of the grains. However, domains had no influence on the reactivity of the other 80% and are therefore secondary to the surface orientation in determining the reactivity.

KEYWORDS

ferroelastic materials, photocatalysis, surface

1 | INTRODUCTION

In an attempt to develop environmentally friendly fuel alternatives, interest has increased in the potential application of photocatalytic materials that use solar energy to split water and produce hydrogen.[1,2] However, because known photocatalysts are too inefficient to produce hydrogen at competitive prices,[3,4] it is important to understand how they can be improved.[5] Morrison detailed the most important characteristics a photocatalyst must exhibit to efficiently split water using sunlight.[6] One important characteristic is the ability to spatially separate the reduction and oxidation reaction sites on the catalyst surface, which decreases the recombination of photogenerated charge carriers and reaction products.[6]

Oxidation and reduction sites can be separated if different areas of the catalyst surface have different surface potentials, which results in relatively more photocathodic and photoanodic regions.[6] Regions of different surface potential might arise from differences in orientation,[7,8] chemical termination,[9-11] or internal polarizations resulting from ferroelectric[12-14] or ferroelastic domains.[15,16] Most of the prior work focused on how a single source of varying surface potential affected reactivity. Pisat et al[17] recently showed that when the influence of both different surface orientations and different chemical terminations on the surfaces of $SrTiO_3$ grains were considered together, surface orientation played the dominant role in determining the reactivity and the chemical termination affected reactivity in a secondary way.

The goal of this study was to determine the relative influence of surface orientation and the ferroelastic domain structure on the photocathodic reactivity of $CaTiO_3$. The surfaces of ferroelastic materials have been shown to have relatively photocathodic and photoanodic sites associated with alternating ferroelastic domains that spatially separate

photogenerated charge carriers.[15,16] Munprom et al[8,15,18] found that on the surface of ferroelastic $BiVO_4$, some ferroelastic domains were found to be reactive for reduction, and the others were active for oxidation. Pisat et al[16] studied the photochemical reactivity of ferroelastic WO_3, which has a more complex domain structure, but also showed spatially selective reactivity. The mechanism that creates spatially selective reactivity on ferroelastic domains is not yet clear, although the flexoelectric effect[15,19] and point defect redistribution have been proposed as possible mechanisms.[20,21]

$CaTiO_3$ was selected for this study because it is ferroelastic[22] and, having a perovskite related structure, is expected to exhibit orientation dependent reactivity similar to what has been documented for $SrTiO_3$.[7,17,23] Above 1250°C, $CaTiO_3$ has the ideal perovskite structure ($Pm\bar{3}m$), in the range of 1250°C to 1000°C it distorts to a tetragonal symmetry ($I4/mcm$), and between 1000°C and room temperature, it adopts an orthorhombic symmetry ($Pcmn$).[24] The lower symmetry structures result from octahedral tilting that alters the cation-anion bond distances, but not the coordination numbers of the ions. The reduction in symmetry that occurs during cooling produces a ferroelastic domain structure that locally reduces the strain associated with the phase transformations.[25] $CaTiO_3$ has a band gap of 3.5 eV, and although this is too wide to absorb visible light, it is suitable for use as a photocatalyst in ultra-violet (UV) light.[26] The band edge positions are also appropriate for the reduction and oxidation of water, and particulate $CaTiO_3$ has shown high photocatalytic activity for the production of H_2.[26,27] More recently, H_2 production from a hierarchically structured $CaTiO_3$ illuminated by visible light has been reported.[28]

2 | METHODS

Polycrystalline $CaTiO_3$ ceramics were created from $CaTiO_3$ powders (99.9%, Alfa Aesar) using conventional processing techniques detailed in the supplemental information. When the polished sample is annealed at 1250°C, it has the cubic structure and noticeable facets are formed on the surface. As it cools to room temperature, the material transforms first to the tetragonal phase, and then to the orthorhombic phase, creating ferroelastic domains.

Following annealing, the surface topography was imaged by atomic force microscopy (AFM), with a Solver-NEXT or an NTEGRA AFM (NT-MDT). The ferroelastic domain structure was imaged in backscattered electron (BSE) contrast using a Quanta 600 (FEI) scanning electron microscope (SEM). The orientations of the grains were determined using electron backscatter diffraction (EBSD), also using a Quanta 600 (FEI) SEM. For both SEM imaging techniques, the acquisition parameters included an accelerating voltage of 20 kV, a spot size of 5 nm, and a 10 mm working distance. For EBSD, the sample was mounted so that the surface was at a 70° angle to the electron beam. EBSD patterns were obtained for each grain and orientations were assigned assuming the cubic $CaTiO_3$ structure. As mentioned earlier, the orthorhombic calcium titanate structure is a slight distortion of the cubic perovskite structure. The pseudo cubic lattice parameters of the orthorhombic calcium titanate structure (3.795, 3.822, and 3.849 Å) differ from the cubic structure by $\leq 1.4\%$. In practice, this makes it a challenge to differentiate the (100), (010), and (001) planes in EBSD patterns. Because of this challenge, and the expected physical similarity of these three planes, we simplified the problem by indexing the orientations in the cubic system. Note that when the facet structure forms at high temperature, the structure is cubic.

The orientations of facets on the surfaces of the grains were determined using the topographic AFM images and the measured grain orientations. A MATLab code[17] was used to extract the geometry from the AFM images and to compute the surface normal in the sample reference frame. The Euler angles specifying the grain's orientation were then used to rotate the surface normal into the crystal frame, specifying the orientation of the facet. Some uncertainty arises in this process because of the finite size of the AFM probe; this uncertainty is greatest for the smallest facets.

Marker reactions were used to identify the locations of photoanodic and photocathodic reactions on the surface.[29,30] When a photocatalytic sample is immersed in a solution bearing appropriate metal cations and illuminated, insoluble reduction or oxidation products will be left at the site of the reaction.[31] To identify reduction sites, $CaTiO_3$ was immersed in a solution of 0.075 mol/L $AgNO_3$ and illuminated with UV light of 150 W for 7 seconds to reduce silver. To identify oxidation sites, the samples were immersed in a solution of 0.030 mol/L $Mn(NO_3)_2{\cdot}4H_2O$ and illuminated with UV light of 210 W for 90 seconds, which produced manganese oxide particles. The reduction and oxidation reactions can be expressed in the following way[30]:

$$Ag^{+}_{(aq)} + e^{-} \rightarrow Ag_{(s)},$$

$$Mn^{2+}_{(aq)} + 2h^{+} + 2H_2O \rightarrow MnO_{2(s)} + 4H^{+}.$$

Following these marker reactions, AFM imaging was used to determine the location of the reaction products. Note that no sacrificial reagents were used in these experiments. Because of this choice, the rates of the reduction and oxidation reactions written above were likely affected by rates of the complementary reactions, which are the oxidation and reduction of water respectively. The rates at which water is oxidized and reduced are of principal interest for the performance of water splitting catalysts. The addition of easily

oxidized or reduced species might have led to different results, more characteristic of the marker reactions.

To quantify the spatial selectivity of the reactivity, the volume of the reaction product was measured by analyzing the topographic AFM images. For this measurement, the image of the surface before the reaction was subtracted from the image of the same area after reaction and the integral height difference provided a measure of the excess volume per surface area that could be compared for different orientations or areas of the surface. In cases where some portion of the bare surface still remains visible after the reaction, two-dimensional height profiles also provide a quantitative assessment of the amount of reaction product on different areas in an image.

3 | RESULTS

Figure 1 compares SEM and AFM images of the same area of the $CaTiO_3$ surface after polishing and annealing. The backscattered electron (BSE) image in Figure 1A shows alternating stripes of light and dark contrast within the grains, created by the different orientations of the ferroelastic domains. Examples of these domains are indicated by the white arrows in the image. Three types of ferroelastic domain boundaries have been identified in $CaTiO_3$. Using the pseudo cubic perovskite indexing, there are 180° boundaries separated by (100) planes, 90° boundaries separated by (100) planes, and 180° boundaries separated by (110) planes.[22,32] It has been reported that the 180° boundaries separated by (100) planes are the most common and that (110) boundaries are not found in artificial crystals.[22,25,32-35] If this is true, the parallel domain walls evident in Figure 3A are most likely (100) domain walls (or (101) in the orthorhombic system). If so, the two darkest V-shaped domains are likely to have been created by other (100) variants.

Figure 1B shows a topographic AFM image of the same area of the surface. Feint striped contrast within the grains represent areas of the surface that are slightly higher and lower and has the same direction and location of the domains seen in Figure 1A. The same domains are labeled with white arrows in both images, where the ferroelastic domains that appear as lighter gray in the BSE image are slightly raised in the AFM image. In Figure 1, there is also evidence of faceting. Higher resolution AFM images show that some surfaces are flat as in Figure S1A (defined as having no steps higher than 3 nm), others have two facets as in Figure S1B, and the remainder have three facets as in Figure S1C.

The observation of faceted surfaces indicates that there are missing orientations in the equilibrium crystal shape.[36] In this case, the equilibrium shape might be made up of a small number of low energy facets. This idea can be tested by indexing the orientation of many of the observed faces and plotting them on a stereogram.[37] This analysis, the details of which have been published previously,[17] is described in more detail in the supplemental information section (see Figures S2 and S3). To determine the facet orientations on $CaTiO_3$, 50 points were accumulated from each of 40 different sets of parallel facets on grains with 30 different orientations. The results are plotted together on the stereogram in Figure 2A and show that the observations are consistent with the model that all surface orientations are replaced by combinations of {001}, {011}, and {111} orientations (pseudo cubic), or orientations close to them. Note that some geometries require two nonparallel {011} type facets, so the stereogram is extended to include a second {011} surface, the $(\bar{1}01)$ plane.

Based on these experimental observations, we constructed a model for the surface, illustrated in Figure 2B, using the conventions established by Cahn and Handwerker.[37] The shaded region around {100} indicates that the {100} orientation and orientations vicinal to {100} are all part of the equilibrium crystal shape. In this part of orientation space, the surfaces are flat. The tie lines indicate orientations that can be constructed from two distinct facets (those at the ends of the tie line). The unshaded areas indicate parts of orientation space that must be constructed of three facets (those at the vertices of the triangular regions). In Figure 2C, the observed surface orientations are colored by the number of facets observed on the surface (the observations are now folded into the standard stereographic triangle for cubic materials because the grain orientations of (011) and $(\bar{1}01)$ are indistinguishable). The criterion for a flat surface was that no steps larger than 3 nm were observed. The observations are consistent with the model, within the expected uncertainty of

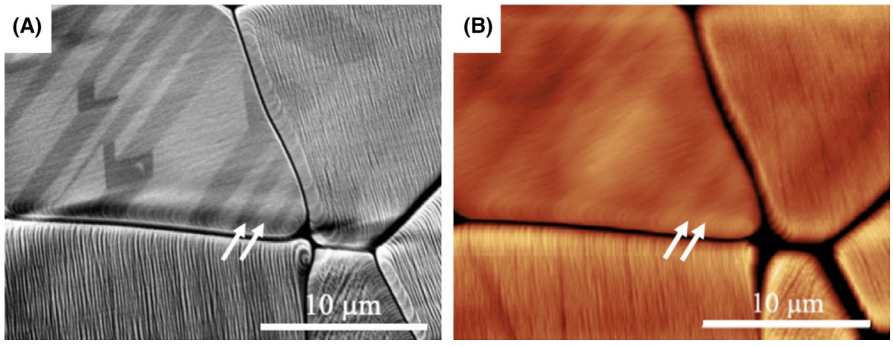

FIGURE 1 Example of the microstructure in the $CaTiO_3$ sample. A, BSE image of several grains following anneal. B, Topographic AFM image of the same area shown in (A). The vertical scale of the topographic image (from dark-to-light) in (B) is 159 nm [Color figure can be viewed at wileyonlinelibrary.com]

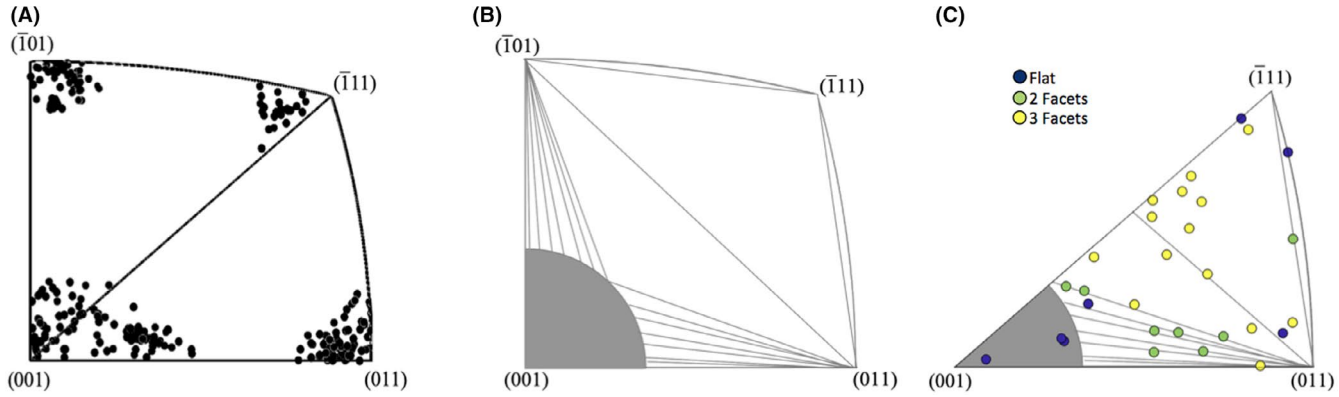

FIGURE 2 A, Orientations of 50 points from 40 sets of facets on the surface of 30 different grains in the $CaTiO_3$ sample. B, Surface model of the $CaTiO_3$ sample. (C) Orientations of 29 grains plotted over the surface model shown in (B), folded into the standard cubic projection [Color figure can be viewed at wileyonlinelibrary.com]

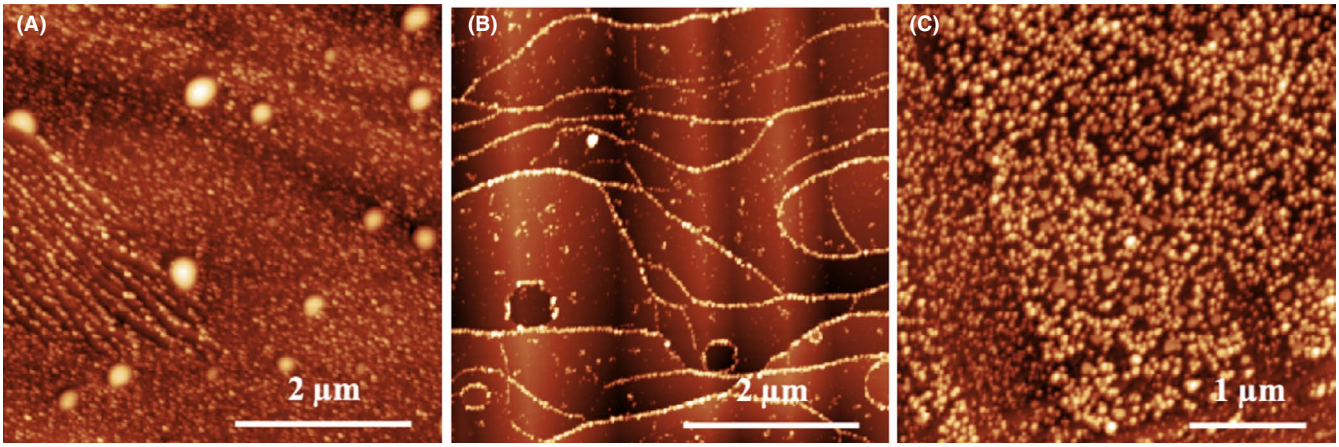

FIGURE 3 Topographic AFM images of an (A) (001) oriented grain, (B) (011) oriented grain, and (C) (111) oriented grain after the silver reduction reaction. AFM images of the same areas, before the reaction, are shown in Figure S5. The vertical scales of the topographic images (from dark-to-light) are: (A) 40.8 nm, (B) 22.6 nm, and (C) 36.2 nm [Color figure can be viewed at wileyonlinelibrary.com]

the orientation measurements. The model makes it possible to identify the facets expected on an arbitrarily oriented surface, and the relative areas of those facets. As a final note, it should be mentioned that it is possible that there is a small range of vicinal surfaces around {111} and {110} (smaller than around {100}), but there was not enough data to confirm or refute that possibility.

AFM imaging, before and after the photocathodic reduction of Ag^+, was used to determine the location of reaction products on the surface. With ceramics samples, there may be some concern that the grain boundaries or thermoelastic strains influence the reactivity. The grain boundaries were not observed to influence the reactivity (see Figure S4). While the thermoelastic strains in the microstructure might influence the domain structure, it does not suppress it, as illustrated in Figure 1 and Figure S4. Topographic AFM images of grains with single facet orientations near {001}, {011}, and {111}, respectively, are shown in Figures S5A-C before reaction, and in Figure 3A-C after the photochemical reduction of silver. The features that appear on the surface after the reaction are reduced silver and by comparing the topographic data in the same area before and after the reaction, it is possible to estimate the amount of silver deposited. In this case, the amounts of silver on the {011}, {001}, and {111} surfaces were 1.05, 2.42, and 6.19 nm^3/nm^2 respectively. Based on these measurements, the {111} orientation is the most reactive and the {011} orientation is the least reactive. For the case of {011}, this is almost certainly an overestimate; note that the reduced silver is found almost exclusively at step edges which locally have a different crystallographic orientation. The amount of silver reduced on a perfectly flat surface would almost certainly be much smaller. These steps form to compensate for local deviations in the orientation from the ideal {011} orientation. The steps most likely have orientations that are near other parts of the equilibrium crystal shape, such as {100} and {111}. Because these other orientations promote the photocathodic reaction, Ag^+ is reduced selectively at these locations.

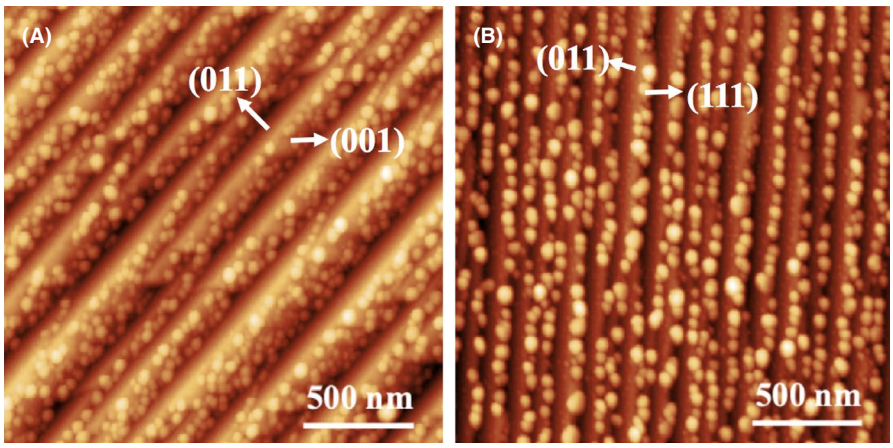

FIGURE 4 Topographic AFM images of grains with (A) one (001) and one (011) set of facets, (B) one set of (111) and one set of (011) facets. The vertical scales of the topographic images (from dark-to-light) are: (A) 90 nm, (B) 56 nm [Color figure can be viewed at wileyonlinelibrary.com]

The topographic variations characteristic of the ferroelastic domain structure are visible in the images shown in Figures S5B,C; in the corresponding images after reduction, it is clear that silver reduced on all domains. In Figure 3C, one set of domains seems to have reduced less silver than the other, but this does not seem to be the case in Figure 3B. To quantify this visual assessment, we can measure the heights of the deposits and the excess volume on the different domains and compare them.

In Figure S5B the ferroelastic domains are clearly visible at the surface of this {011} oriented grain, extending vertically from the top to bottom of the image. Figure S6 shows the same area of this grain, following the silver reduction reaction. As noted above, the amount of silver does not appear to vary with the domains. The square outlined by the green dashed line in Figure S6A shows the area used to calculate the volume of silver on the lower domain and the square outlined by the blue solid line shows the area used to calculate the volume of silver on the higher domain. The volumes of silver on the lower and higher domains were 1.29 and 1.37 nm^3/nm^2 respectively. This 5% difference is not believed to exceed the uncertainty of the measurement. This result is further supported by height profiles taken from the AFM image of the reacted surface. The locations of the heights profiles in Figure S6B are shown in Figure S6A by the dashed green and solid blue lines. While one domain is physically higher than the other, the differences in height between the silver and the surface are about the same for each, indicating that both domains have about the same reactivity.

Figure S7 shows a different area of the {111} oriented grain shown in Figure 3C. Figure S7A is an AFM image of the surface of the grain before the reaction, and Figure S7B shows the same area of the surface after the photocathodic reduction of Ag^+. The ferroelastic domains in this grain can be seen in Figure S7A as stripes extending diagonally across the image. Visually, it is clear that the amount of silver deposited on each domain is not uniform. The volume of silver on the topographically lower (higher) set of domains in the area marked by the box with the green dashed (blue solid) line in Figure S7B is 3.37 nm^3/nm^2 (7.81 nm^3/nm^2). Therefore, one set of domains has more than twice the amount of silver as the other. The height profiles plotted in Figure S7C, along the lines marked in Figure S7B, are consistent with the volume measurement because the heights of the silver deposits on the topographically higher domain (marked by the solid blue line) are larger than on the other domain (marked by the green dashed line). When we compare this to the findings for the {011} orientated grain discussed above, it is clear that, while grains with some orientations show spatially selective reactivity that correlates with the domain structure, not all orientations show the same phenomenon. For the grains without spatially selective reactivity, it is possible that the domains do not create sufficient polarization perpendicular to those surface orientations.[38]

For arbitrarily oriented grains whose surfaces are made up of two or three facets, the reactivity is nonuniform, with some of the facets being more reactive than others. Examples illustrating this phenomenon are shown in Figure 4 and Figure S8. The orientations of the reactive and unreactive facets were determined for each of these grains, and are indicated in the images. In every case, the facets reactive for reduction have either the {001} or {111} orientation, and the unreactive facets are {011} surfaces. Among the arbitrarily oriented grains studied, there are examples where spatial selectivity is correlated with the domain structure on some grains, but other cases where the reactivity is uniform and independent of the domain structure.

Recall that for an arbitrarily oriented surface, the geometry and relative areas of the surface facets can be predicted based on the surface model illustrated in Figure 2B. Using this model, one can hypothesize that if we assign a magnitude of reactivity to each facet orientation, then the reactivity of an arbitrarily oriented surface is equal to the linear combination of those reactivities weighted by the relative areas of the facets. For the relative reactivities of the three facet orientations, we will use the measurements for the three grains with near {001}, {011}, and {111} orientations, illustrated in Figure 3. Recognizing the uncertainty in the measurements

of the excess volume of silver, we approximated the observed values of 1.05, 2.42, and 6.19 nm^3/nm^2 as 1, 2.5, and 6 nm^3/nm^2 for the {011}, {100}, and {111} oriented surfaces respectively.

The orientation and reactivity were measured for 29 grains and these results are summarized in Figure S9. The color of each point in the plot corresponds to the reactivity of the grain, measured in nm^3 of silver per nm^2 area of surface, the value of which is indicated by the color bar in the figure. When the reactivity is predicted based on the area-weighted reactivities of the flat facets, the results in Figure S9B are obtained. The graph in Figure 5 compares the observed and predicted reactivities for each grain. The solid black line marks the points at which the observed value is equal to the predicted value, so points above the line represent grains with reactivities that are observed to be higher than predicted, and those below the line have reactivities lower than the predicted value. Grains represented by a green diamond had reactivity that was spatially selective and correlated with either the facet orientation or ferroelastic domain structure, and grains represented by blue squares had spatially uniform reactivity.

To locate the oxidation sites on the surface, a marker reaction that oxidizes Mn^{2+} in solution to solid MnO_x on the surface was used. Figure 6A shows the surface of a grain with {001} and {011} facets, prior to any reaction, Figure 6B shows the same area after silver reduction, and Figure 6C shows the same surface following the Mn oxidation reaction. It can be seen in these images that the {011} facets, which are not reactive for reduction, have MnO_x particles on their surface, and are therefore active for oxidation. However, the two reactions are not completely complementary. The {001} orientation and the junctions between the two facets, which are active for reduction, also appear to have some activity for oxidation.

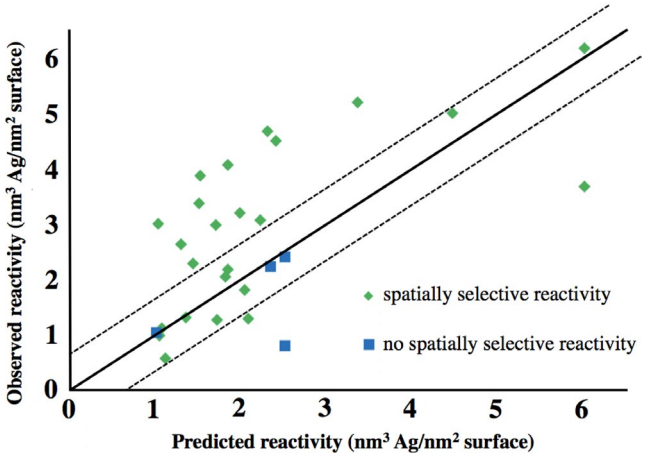

FIGURE 5 Graph of the experimentally observed amount of reduced Ag compared to that predicted based on the reactivity of the low index faces and their relative areas [Color figure can be viewed at wileyonlinelibrary.com]

4 | DISCUSSION

The results presented here show that the photocathodic reactivity of $CaTiO_3$ surfaces varies strongly with the surface orientation. An earlier study that photo deposited Ag on $CaTiO_3$ particles noted that Ag^+ was selectively reduced on certain facets, but did not determine the orientations.[39] The current work finds that grains of {111} orientation are the most reactive for reduction, and those with orientations near {001} were also reactive for reduction. However, surfaces close to the {011} orientations were almost inert for reduction. For arbitrarily oriented surfaces that are made up of facets, {001} or {111} facets were reactive for reduction, and {011} facets were unreactive for reduction but active for oxidation. This implies a greater surface potential and a greater amount of upward band bending for the {011} surface. The greater upward band bending draws holes to the surface to promote oxidation while slowing the transport of electrons to the surface, which inhibits the reduction reaction.[38] These results show some similarity to results from $SrTiO_3$, which has the ideal perovskite structure and has been studied in greater detail.[9-11,17,23,40] For $SrTiO_3$, all of the past studies agree that {001} is the most reactive for reduction and that {011} is the most reactive for oxidation. Most studies of the reactivity of {111} surfaces have been on single crystals, and this surface has proven to be capable of oxidizing or reducing, depending on its preparation.[9-11] It is interesting to note that the model for the surface structure of $CaTiO_3$ is similar to that determined for $SrTiO_3$ annealed at 1200°C.[7] Furthermore, we observed no evidence that $CaTiO_3$ surfaces that are distinct in the orthorhombic system, but equivalent in the cubic system, had different reactivities.

A comparison of observed reactivities and those predicted by considering the reactivities of the component facets was presented in Figure 5. For the points falling along the black line, or within the uncertainty limits marked by the dashed lines, there is not a significant difference between the observed and predicted reactivity of the grain. Most of the points which lie outside of this region fall above the line, demonstrating that the observed reactivity of the grain is higher than the value predicted through a linear combination of the reactivity of the component facets. It is noteworthy that all of these points are on grains where there is some spatial separation of the reaction sites. This suggests that the spatial separation of photocathodic and photoanodic sites increases the reactivity beyond that expected from the component facets alone. In cases where there are step edges, there might also be an enhanced contribution from those steps. However, the difference between the observed and predicted reactivity for these grains decreases as the predicted reactivity increases and is never more than double the predicted reactivity. Therefore, if the spatial separation of photocathodic and photoanodic sites on the faceted surfaces increases the reactivity of the grains,

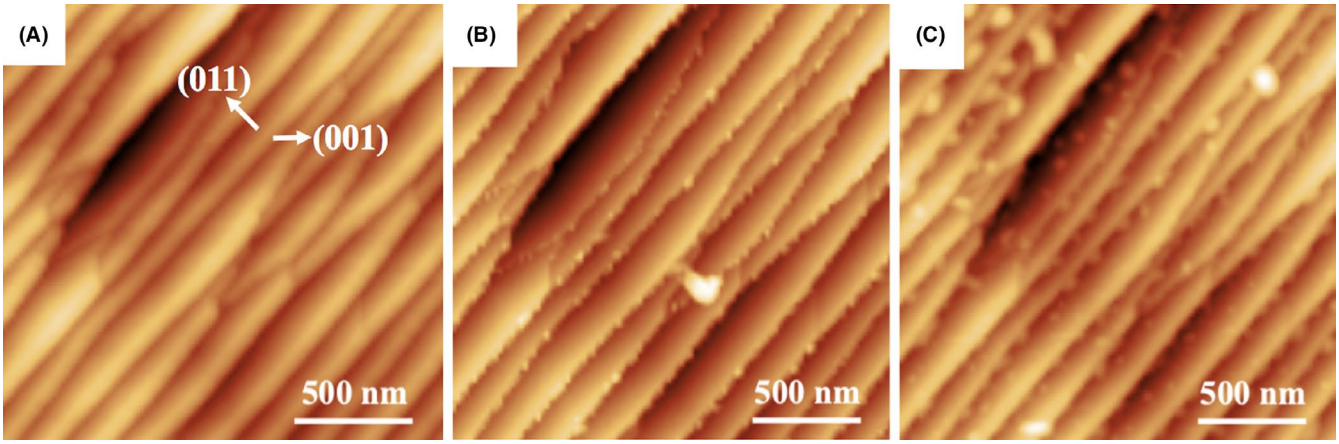

FIGURE 6 Topographic AFM images of the same surface (A) before marker reactions, (B) following the silver reduction reaction, and (C) after the manganese oxidation reaction. The vertical scales of the topographic images (from dark-to-light) are: (A) 32.0 nm, (B) 35.8 nm, (C) 31.0 nm [Color figure can be viewed at wileyonlinelibrary.com]

it is not by a factor of more than two. Finally, it should be noted that even on the surfaces designated as 'flat', spatial selectivity is not completely eliminated. For example, the step edges on the {011} surface (See Figure 3B) provide some separation of charge, even though this was classified as a surface without facets and spatial selectivity.

Figure 6 shows that the {011} surface is completely unreactive for reduction but active for oxidation, and the {001} surface is bifunctional; it can reduce silver and oxidize manganese. This might explain why the impact of having complementary photocathodic and photoanodic domains does not increase the reactivity more significantly. The bifunctionality of the {001} surface means that charge carrier separation is not a requirement for the complete reaction to proceed. Therefore, adding {011} facets with more photoanodic sites may not have as significant an influence on the overall reaction rate as expected.

The influence of the ferroelastic domain structure on the reactivity was obvious only on selected grains and, even when it was obvious, was less influential than the surface orientation. $CaTiO_3$ has also been reported to be ferroelectric when subjected to sufficient strain,[41,42] but this level of strain (1.5%) is not expected in a polycrystal, so it is unlikely that a ferroelectric phase in some of the grains could account for observations. It should also be noted that the existence of this ferroelectric phase remains the subject of debate.[43] While the ferroelastic domain boundaries themselves have been reported to be polar,[44-46] in no circumstances were the boundaries alone observed to be more or less reactive than the nearby surfaces. In fact, the influence of the ferroelastic domains in $CaTiO_3$ on the photochemical reactivity appears to be much smaller than for WO_3 and $BiVO_4$.[15-16,18] One possibility is that the differences in the surface potentials between the facets of different orientation are greater in $CaTiO_3$ than for the previously studied cases, and this overwhelms the influence of the domains. It is also possible that the domains in $CaTiO_3$ do not separate charge as well as WO_3 and $BiVO_4$. One significant difference between the domains in these materials is their typical sizes. Both WO_3 and $BiVO_4$ had domains a few hundred nanometers in width,[15,16] while those in $CaTiO_3$ are typically several times larger. It is possible that the larger domain size makes it more difficult to separate carriers because they have to be transported over greater distances. Calculations for $BaTiO_3$ have shown that photochemical reactivity is optimized at a domain size of about 200 nm, and reactivity then decreases for larger domains.[47]

Another way that $CaTiO_3$ differs from $BiVO_4$ and WO_3 that might contribute the reduced influence of the domain structure on the reactivity is the absence of the anti-ferroelectric state found in the latter two compounds.[15-16,18] Both $BiVO_4$ and WO_3 are anti-ferroelectric and both have a ferroelectric phase below room temperature; neither statement is true for $CaTiO_3$.[19] Anti-ferroelectric materials generally exhibit a large coupling constant between the polarization and magnitude of the strain gradient in the material, and these types of materials often have a higher potential to form polar units.[19] Therefore, it is possible that this allows the surfaces of these materials to form a strong polar state corresponding to the ferroelastic domain structure, contributing to the spatial separation of photoanodic and photocathodic reaction sites. Finally, if the polarity of the ferroelastic domains has its origin in the partitioning of charged point defects,[20] and $CaTiO_3$ is closer to an ideal stoichiometry than $BiVO_4$ and WO_3, then this would lead to smaller polar charges which would be consistent with the reduced spatial selectivity of the reduction reaction.

5 | CONCLUSIONS

Arbitrarily oriented $CaTiO_3$ surfaces, when annealed in air at 1250°C, are made up of combinations of flat facets with orientations near {001}, {011}, and {111} (using pseudo cubic

symmetry). The photochemical reactivity of $CaTiO_3$ shows a significant dependence on the surface orientation. Surfaces with the {111} orientation are the most active for reduction, followed by those with orientations near {001}, and grains with {011} orientations are the least reactive. The {011} orientations are active for oxidation. When {011} facets are present on the same surface with {111} or {001} facets, the photocathodic reduction reaction happens exclusively on the {111} or {001} facets. In some cases, the spatial selectivity of the reaction corresponds to the pattern of ferroelastic domains. However, this was not true in all cases where domains were observed. Overall, the photochemical reactivity of $CaTiO_3$ is mostly determined by the surface orientation and the ferroelastic domain structure has a smaller influence.

ACKNOWLEDGMENTS

The authors acknowledge the support of National Science Foundation grant DMR 1609369 and use of the Materials Characterization Facility at Carnegie Mellon University supported by grant MCF-677785.

ORCID

Paul A. Salvador https://orcid.org/0000-0001-7106-0017
Gregory S. Rohrer https://orcid.org/0000-0002-9671-3034

REFERENCES

1. Fujishima A, Honda K. Electrochemcial photolysis of water at a semiconductor electrode. Nature. 1972;238(5358):37–8.
2. Osterloh FE. Inorganic nanostructures for photoelectrochemical and photocatalytic water splitting. Chem Soc Rev. 2013;42(6):2294–320.
3. Pinaud BA, Benck JD, Seitz LC, Forman AJ, Chen Z, Deutsch TG, et al. Technical and economic feasibility of centralized facilities for solar hydrogen production via photocatalysis and photoelectrochemistry. Energy Environ Sci. 2013;6(7):1983–2002.
4. Sathre R, Scown CD, Morrow WR, Stevens JC, Sharp ID, Ager JW, et al. Life-cycle net energy assessment of large-scale hydrogen production via photoelectrochemical water splitting. Energy Environ Sci. 2014;7(10):3264–78.
5. Acar C, Dincer I, Naterer GF. Review of photocatalytic water-splitting methods for sustainable hydrogen production. Int J Energy Res. 2016;40(11):1449–73.
6. Morrison SR. Electrochemistry at Semiconductor and Oxidized Metal Electrodes. New York, NY: Plenum Press; 1980.
7. Giocondi JL, Rohrer GS. Orientation dependence of photochemical reduction reactions on $SrTiO_3$ surfaces. Mater Res Soc Proc; 2003. Pittsburgh, PA.
8. Munprom R, Salvador PA, Rohrer GS. The orientation dependence of the photochemical reactivity of $BiVO_4$. J Mater Chem A. 2015;3(5):2370–7.
9. Giocondi JL, Rohrer GS. Structure sensitivity of photochemical oxidation and reduction reactions on $SrTiO_3$ surfaces. J Am Ceram Soc. 2003;86(7):1182–9.
10. Zhu Y, Salvador PA, Rohrer GS. Controlling the relative areas of photocathodic and photoanodic terraces on the $SrTiO_3$(111) surface. Chem Mater. 2016;28(14):5155–62.
11. Zhu YS, Salvador PA, Rohrer GS. Controlling the termination and photochemical reactivity of the $SrTiO_3$(110) surface. Phys Chem Chem Phys. 2017;19(11):7910–8.
12. Giocondi JL, Rohrer GS. Spatially selective photochemical reduction of silver on the surface of ferroelectric barium titanate. Chem Mater. 2001;13(2):241–2.
13. Kalinin SV, Bonnell DA, Alvarez T, Lei X, Hu Z, Ferris JH, et al. Atomic polarization and local reactivity on ferroelectric surfaces: a new route toward complex nanostructures. Nano Lett. 2002;2(6):589–93.
14. Schultz A, Zhang Y, Salvador P, Rohrer G. Effect of crystal and domain orientation on the visible-light photochemical reduction of Ag on $BiFeO_3$. ACS Appl Mater Interfaces. 2011;3(5):1562–7.
15. Munprom R, Salvador PA, Rohrer GS. Polar domains at the surface of centrosymmetric $BiVO_4$. Chem Mater. 2014;26(9):2774–6.
16. Pisat AS, Rohrer GS, Salvador PA. Spatial selectivity of photodeposition reactions on polar surfaces of centrosymmetric ferroelastic gamma-WO_3. J Mater Chem A. 2017;5(18):8261–6.
17. Pisat AS, Salvador PA, Rohrer GS. The facet structure and photochemical reactivity of arbitrarily oriented strontium titanate surfaces. Adv Mater Interfaces. 2019;6(16):1900731.
18. Munprom R, Salvador PA, Rohrer GS. Ferroelastic domains improve photochemical reactivity: a comparative study of monoclinic and tetragonal $(Bi_{1-0.5x}Na_{0.5x})(V_{1-x}Mo_x)O_4$ ceramics. J Mater Chem A. 2016;4(8):2951–9.
19. Pisat AS, Rohrer GS, Salvador PA. Spatially selective photochemical activity on surfaces of ferroelastics with local polarization. Semicond Sci Technol. 2017;32(10):103001.
20. Kim Y, Morozovska AN, Kumar A, Jesse S, Eliseev EA, Alibart F, et al. Ionically-mediated electromechanical hysteresis in transition metal oxides. ACS Nano. 2012;6(8):7026–33.
21. Li Q, Lu T, Schiemer J, Laanait N, Balke N, Zhang Z, et al. Giant thermally-enhanced electrostriction and polar surface phase in $La_2Mo_2O_9$ oxygen ion conductors. Phys Rev Mater. 2018;2(4):041403(R).
22. Kay HF, Bailey PC. Structure and properties of $CaTiO_3$. Acta Cryst. 1957;10(3):219–26.
23. Mu L, Zhao Y, Li A, Wang S, Wang Z, Yang J, et al. Enhancing charge separation on high symmetry $SrTiO_3$ exposed with anisotropic facets for photocatalytic water splitting. Energy Environ Sci. 2016;9(7):2463–9.
24. Yashima M, Ali R. Structural phase transition and octahedral tilting in the calcium titanate perovskite $CaTiO_3$. Solid State Ionics. 2009;180(2–3):120–6.
25. Wang YB, Liebermann RC. Electron-microscopy study of domain-structure due to phase-transitions in natural perovskite. Phys Chem of Miner. 1993;20(3):147–58.
26. Mizoguchi H, Ueda K, Orita M, Moon S-C, Kajihara K, Hirano M, et al. Decomposition of water by a $CaTiO_3$ photocatalyst under UV light irradiation. Mater Res Bull. 2002;37(15):2401–6.
27. Wang RN, Ni S, Liu G, Xu XX. Hollow $CaTiO_3$ cubes modified by La/Cr co-doping for efficient photocatalytic hydrogen production. Appl Catal B Environ. 2018;225:139–47.
28. Pei J, Meng J, Wu S, Lin Q, Li J, Wei X, et al. Hierarchical $CaTiO_3$ nanowire-network architectures for H_2 evolution under visible-light irradiation. J Alloys Compd. 2019;806:889–96.
29. Tanaka K, Harada K, Murata S. Photocatalytic deposition of metal-ions onto TiO_2 powder. Sol Energy. 1986;36(2):159–61.

30. Wenderich K, Mul G. Methods, mechanism, and applications of photodeposition in photocatalysis: a review. Chem Rev. 2016;116(23):14587–619.
31. Herrmann JM, Disdier J, Pichat P. Photocatalytic deposition of silver on powder titania - consequences for the recovery of silver. J Catal. 1988;113(1):72–81.
32. Bowman HL. On the structure of perovskite from the Burgumer Alp, Pfitschthal, Tyrol. Miner Mag J Miner Soc. 1908;15(69):156–76.
33. Pramanik S, Ravikumar K, Kalsar R, Suwas S, Basu B. On the orientation relationships in phase transformation of $CaTiO_3$. Ceram Int. 2019;45(9):12509–15.
34. Van Aert S, Turner S, Delville R, Schryvers D, Van Tendeloo G, Salje EKH. Direct observation of ferrielectricity at ferroelastic domain boundaries in $CaTiO_3$ by electron microscopy. Adv Mater. 2012;24(4):523–7.
35. White TJ, Segall RL, Barry JC, Hutchinson JL. Twin boundaries in perovskite. Acta Cryst B. 1985;41(2):93–8.
36. Herring C. Some theorems on the free energies of crystal surfaces. Phys Rev. 1951;82(1):87–93.
37. Cahn JW, Handwerker CA. Equilibrium geometries of anisotropic surfaces and interfaces. Mater Sci Eng A. 1993;162(1–2):83–95.
38. Song WJ, Salvador PA, Rohrer GS. Influence of the magnitude of ferroelectric domain polarization on the photochemical reactivity of $BaTiO_3$. ACS Appl Mater Interfaces. 2018;10(48):41450–7.
39. Anzai A, Fukuo N, Yamamoto A, Yoshida H. Highly selective photocatalytic reduction of carbon dioxide with water over silver-loaded calcium titanate. Catal Comm. 2017;100:134–8.
40. Giocondi JL, Salvador PA, Rohrer GS. The origin of photochemical anisotropy in $SrTiO_3$. Topics Catal. 2007;44(4):529–33.
41. Haislmaier RC, Lu YF, Lapano J, Zhou H, Alem N, Sinnott SB, et al. Large tetragonality and room temperature ferroelectricity in compressively strained $CaTiO_3$ thin films. APL Mater. 2019;7(5):051104.
42. Sarantopoulos A, Ong WL, Malen JA, Rivadulla F. Effect of epitaxial strain and vacancies on the ferroelectric-like response of $CaTiO_3$ thin films. Appl Phys Lett. 2018;113(18):182902.
43. Steciuk G, David A, Petricek V, Palatinus L, Mercey B, Prellier W, et al. Precession electron diffraction tomography on twinned crystals: application to $CaTiO_3$ thin films. J Appl Cryst. 2019;52:626–36.
44. Nataf GF, Guennou M, Kreisel J, Hicher P, Haumont R, Aktas O, et al. Control of surface potential at polar domain walls in a nonpolar oxide. Phys Rev Mater. 2017;1(7):074410.
45. Yokota H, Niki S, Haumont R, Hicher P, Uesu Y. Polar nature of stress-induced twin walls in ferroelastic $CaTiO_3$. AIP Adv. 2017;7(8):085315.
46. Zhao Z, Barrett N, Wu Q, Martinotti D, Tortech L, Haumont R, et al. Interaction of low-energy electrons with surface polarity near ferroelastic domain boundaries. Phys Rev Mater. 2019;3(4):043601.
47. Glickstein JJ, Salvador PA, Rohrer GS. Multidomain simulations of coated ferroelectrics exhibiting spatially selective photocatalytic activity with high internal quantum efficiencies. J Mater Chem A. 2016;4(41):16085–93.

SUPPORTING INFORMATION

Additional supporting information may be found online in the Supporting Information section.

How to cite this article: Zitello KE, Salvador PA, Rohrer GS. Influence of surface orientation on the photochemical reactivity of $CaTiO_3$. *J Am Ceram Soc*. 2020;103:4498–4506. https://doi.org/10.1111/jace.17107